Proceedings of the 2016 Manufacturing Science and Engineering Conference
MSEC2016
June 27-July 1, 2016, Virginia Tech, Blacksburg, USA

MSEC2016-8767

MESO-SCALE DIGITAL MATERIALS: MODULAR, RECONFIGURABLE, LATTICE-BASED STRUCTURES

Benjamin Jenett
Center for Bits and Atoms, MIT
Cambridge, MA, USA

Daniel Cellucci
Department of Mechanical Engineering,
Cornell University, Ithaca, NY, USA

Christine Gregg
Department of Mechanical Engineering, UC Berkeley
Berkeley, CA, USA

Kenneth Cheung
NASA Ames Research Center
Moffett Field, CA, USA

ABSTRACT

We present a modular, reconfigurable system for building large structures. This system uses discrete lattice elements, called digital materials, to reversibly assemble ultralight structures that are 99.7% air and yet maintain sufficient specific stiffness for a variety of structural applications and loading scenarios. Design, manufacturing, and characterization of modular building blocks are described, including struts, nodes, joints, and build strategies. Simple case studies are shown using the same building blocks in three different scenarios: a bridge, a boat, and a shelter. Field implementation and demonstration is supplemented by experimental data and numerical simulation. A simplified approach for analyzing these structures is presented which shows good agreement with experimental results.

INTRODUCTION

The appeal of a reconfigurable system is that it can perform multiple functions with a base set of parts, rather than requiring multiple systems for multiple functions [1]. Typical to these systems is modularity, which can be desirable for simplification of processes and reduction of part variety [2]. Repetition of modulare elements is something found in periodic frameworks, such as lattice-based cellular structures exhibit high specific stiffness while maintaining lower mass than monolithic structures [3].

Modularity is a fairly ubiquitous trait across multiple scales and industries, including robotics, civil engineering, and aerospace. The Eiffel Tower is made from hierarchical modules- trusses of trusses [4]. Regular space frames were developed as tetrahedral kite structures by Alexander Graham Bell and made popular as “Bucky Domes” by Buckminster Fuller [5]. These strategies make it easy to approximate any form at a desired resolution and allows straight-forward industrial mass production of building components. As we will see, this also allows for potentially simplified repair and reconfiguration. Trusses and space frames are modular, and can be decomposed into struts and nodes- with applications ranging from architecture to solar arrays.

The ability to reconfigure can come from internal mechanisms that allow shape change and reorientation, such as morphing or folding, or from the ability to disassemble a structure into smaller elements and to re-assemble these into another configuration. Examples of morphing structures include soft pneumatic robots [6], actuated compliant wing structures [7], and human-friendly gripping devices [8]. The degree of reconfiguration is typically limited by the ultimate strain of the compliant material changing shape. In quasi-static structures, folding or expanding mechanisms allow reconfiguration of rigid structures with links, pivots, and hinges [9]. Static structures can be reconfigured by robots that climb and manipulate trusses [10], or passive structure modules can be assembled by a specialized assembler robot [11]. Actuation can be encapsulated in the rigid unit itself, resulting in modular, reconfigurable robotic systems. Examples include self-soldering self-reconfiguring modular robot cubes [12], a homogeneous modular robot with locomotion and reconfiguration ability for adaptive furniture [13], and an automated system of self-reconfiguring polyhedral units [14]. The appeal of discrete reconfiguration, as opposed to global shape change, is a higher degree of control and variety in the possible shapes achieved.

Lattice-based structures are found in nature where a high stiffness to weight ratio is advantageous, such as bone or wood [15]. This performance is achieved through the geometric configuration and sparse distribution of material, in contrast to monolithic structures. These properties can be reproduced in man-made materials, such as engineered foams. Due to difficulty in manufacturing these complex geometries with traditional processes, additive manufacturing such as projection micro-stereolithography is used to create millimeter-scale bending and stretch dominated lattice structures with polymers, metals, and ceramics [16].

Another approach is discrete lattice assembly[17]. In this method, planar elements are mechanically linked in 3D to form reversibly assembled composite lattices. This process is not limited by scale, and can be disassembled and reconfigured into other geometries. Previous work has shown that when an axial stretch-dominated geometry with oriented carbon fiber loops is created, the result is a cellular lattice structure with near ideal specific modulus scaling [17]. In addition to mechanical properties, these discrete structures allow simplification of analysis and simulation. Typical time and computation-intensive finite element analysis (FEA) requires meshing of complex geometries [18]. In contrast, the properties of an assembly of building blocks can be predicted from the behavior of its parts. At each level of hierarchy, parts are modeled as discrete finite elements, and as a result the linear system produced for the entire structure can be orders of magnitude smaller than by traditional methods [19].

The possibilities afforded by modular, reconfigurable, high performance structures could have applications in infrastructure or emergency response, as well as implications for how large structures are built on earth or in space. Specifically, it is important for this system to demonstrate flexibility in various different structural morphologies with different structural behaviors, all from the same base elements. Digital materials are presented as modular, reconfigurable, structures with the additional benefits of simplified analysis, scalable multi-functionality, and potential for automated assembly. For this paper, we will investigate a scenario with the following structural morphologies and behaviors: a beam in bending, a plate in compression, and a shell in compression and tension. These take the form of simple macro-scale structures which are, respectively: a bridge, a boat, and a shelter, all built with the same kit of digital material building block parts. We will also show experimental testing of a bench top version to determine bending stiffness, which will be used for comparison to applications where lightweight, stiff structures are needed, specifically, space structures

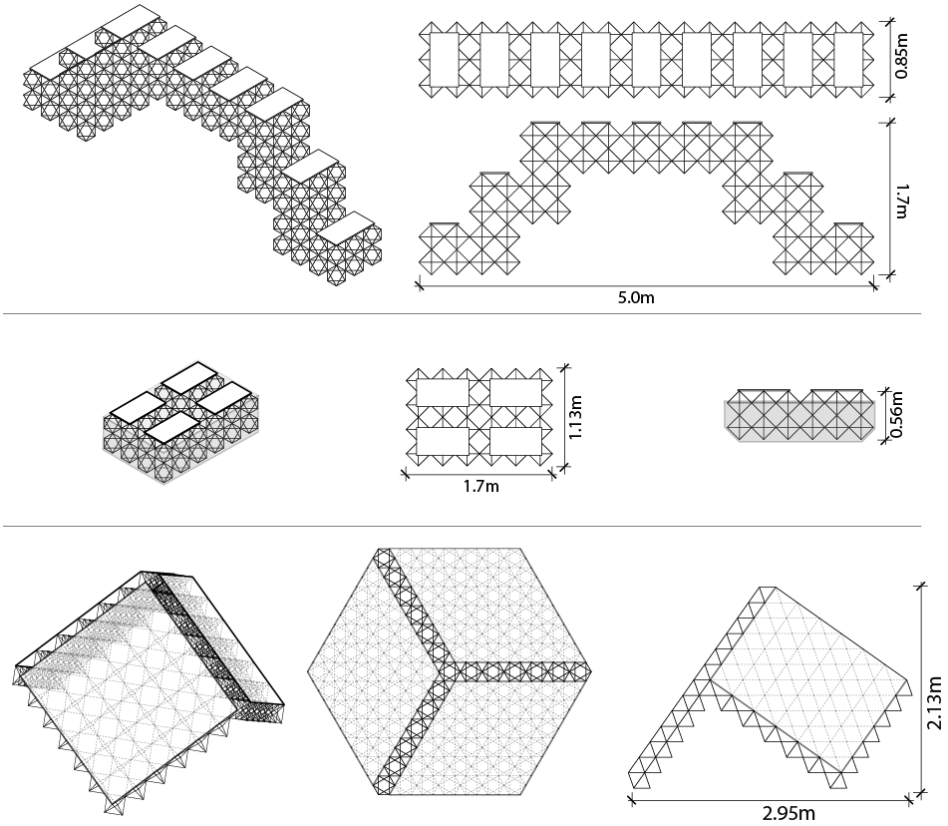

FIGURE 1: OVERVIEW OF DIGITAL MATERIAL STRUCTURE CASE STUDIES. (TOP TO BOTTOM) BRIDGE, BOAT, SHELTER, SHOWING AXONOMETRIC, TOP AND SIDE VIEWS.

METHOD

The digital material construction system consists of modular building blocks which can be attached together to form larger structures of arbitrary size and shape.

Construction System

The primary components of the digital material construction system are struts and nodes. These are assembled to make voxels, which are then used as modular building blocks to build lattice structures.

The struts are conventional commercial pultruded carbon fiber rods (OD: 5mm, ID: 3mm). They are cut to length (175 mm), with an error tolerance of 0.05mm. The material and geometric properties of the struts influence the design of the structure as a result of their mechanical properties. Strut orientation is enforced with internal pockets and strut end caps. The end caps are adhered onto the end of the struts with Loctite Hysol E-120HP (30 N/mm^2 shear strength). This end cap is then captured between the top and bottom node parts, which mate together with snap fit features. This allows voxels to be constructed and deconstructed. Once captured in the interior pockets, the end cap provides resistance to tension forces and prevents strut pullout (FIGURE 4).

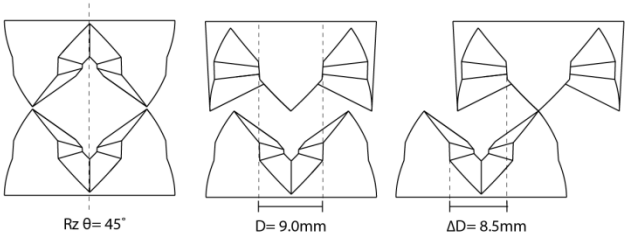

FIGURE 2: HIRTH GEOMETRY. ROTATIONAL AND LATERAL OFFSETS CAN BE COMPENSATED FOR BY NODE GEOMETRY.

The node design satisfies several requirements. The primary function of the nodes is to capture and orient the struts properly, in order to successfully assemble regular octahedra. This is accomplished through the internal geometry of the node (FIGURE 4). Next, voxel to voxel orientation is considered. Proper alignment and orientation is ensured by the node tip geometry, which is a genderless, rotationally symmetric hirth coupling. The hirth coupling is chosen due to its ability to transfer moment (minimum two serrated faces and a bolt fixing them together) as well as the ability to self-center. It has a rotational correction tolerance of 45^o, meaning, regardless of what the orientation of two mating nodes, they will self-center (rotationally). Lateral offset misalignment is also addressed by the serrated hirth design. As shown in FIGURE 2, for tooth width of 9mm, a lateral offset of 8.5mm can be accommodated.

Nodes are manufactured with conventional injection molding of 33% fiber reinforced nylon (Zytel). This material has a Young's Modulus of 9.5 GPa.

We next consider load transfer between voxels. Node to node joints are reversibly fastened with a stainless steel 10-32 screw with a nylon locknut which can take axial tension in the (+X) direction (FIGURE 4). Compression (-X) is handled by face contact between the node and the strut cap, and then the node to its neighbor. Shear in *Y* and *Z*, as well as rotation *Y* and *Z*, are handled primarily by the screw and the cross sectional area of the node hirth. This hirth, designed with four teeth, rotated 22.5^o from orientation of the struts to enable one part to connect with itself, handles the remaining rotation *X*.

TABLE I. VOXEL MASS PROPERTIES

Item	Mass
Bolts (Qty: 3)	12.7g
Nuts (Qty: 3	4.56g
Node hirth (Qty: 6)	34.75g
Node bottom (Qty: 6)	16.8g
Struts (Qty: 12)	46.17g
TOTAL	114.98g

Given the geometry of the voxel, the bounding volume is 0.0227 m^3, with a specific density of 5.056 kg/m^3. A structure built from these voxels will be 99.7% air.

Structure Design

In order to ensure efficient behavior as a structure, certain relationships must be enforced locally, between the strut, the node, and the voxel. The structure must be governed by the behavior of the struts, meaning they must fail by buckling in compression before any part of the node fails, including the strut end cap. Given a nominal load, *P*, applied normal to a node, and assuming fully constrained boundary conditions (ie: full lattice assembly in all directions), each strut will have a load of approximately *0.35*P* or $(P\sqrt{2})/4$) in either tension or compression, depending on its orientation (FIGURE 3). This can be seen below based on the octahedral voxel geometry.

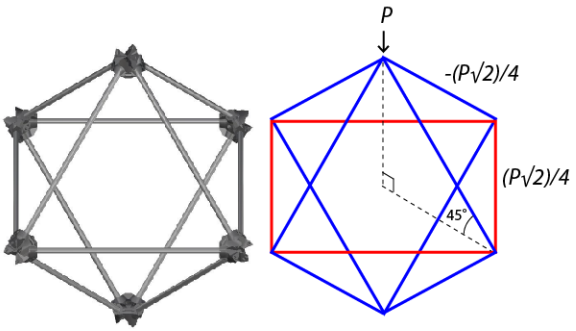

FIGURE 3: VOXEL LOAD TRANSFER. BLUE= COMPRESSION, RED = TENSION

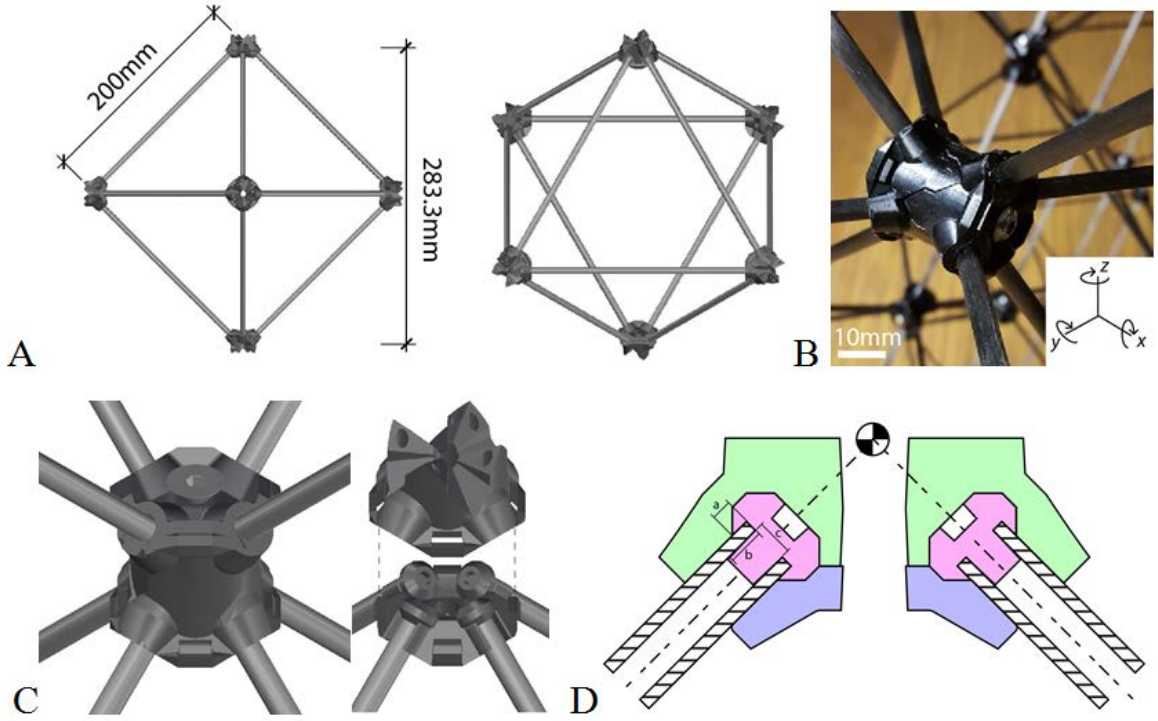

FIGURE 4: VOXEL DETAILS. A- OVERALL DIMENSIONS. B- VOXEL JOINT WITH COORDINATE SYSTEM. C- (L) NODES ASSEMBLED WITH HARDWARE; (R) INTERNAL VIEW OF STRUT ORIENTATION POCKETS AND STRUT END CAPS. D- NODE CROSS SECTION. GREEN = NODE HIRTH, PINK= STRUT CAP, BLUE = NODE BOTTOM; DASHED LINE = CENTROID OF STRUT.

This means that, for a given strut geometry and material, we can determine the buckling load, and therefore the minimum required capacity of the node, which has several different components, each of which will be addressed here.
First, for a first order estimation of the buckling load of a strut, we use simple Euler buckling. Given L= 175mm, E= 130 GPa, and K= 1, we determine P = 1.089 kN. Using this we design the other structural connections withstand loads higher than 1.089 kN.

The areas of contact for the adhesive will give us a tensile capacity for this joint. As shown in FIGURE 4, the contact areas give a surface area of 51.85 mm^2. The adhesive has a shear strength of 30 N/mm^2, which results in 1.53 kN.

The node leg has a cross sectional area of 7mm^2. The material has a tensile stress yield value of 200 MPa, giving a load capacity of 1.4 kN. This is the weakest location in the case of tensile load, but for a given external load, it will still be greater than the buckling load of the struts by 0.311 kN or 22% of its tensile capacity.

The struts with end caps are tested on a uniaxial load testing machine to validate these assumptions. Tension testing, using fixturing to resemble the loading a node would impart on the end cap, results in an average failure load of 4 kN. Compression testing results in an average buckling load of 2.224 kN. There is a large discrepancy between the experimental and analytical buckling predictions. This can be attributed to the boundary conditions. A circle profile matching the strut cross section was milled into a mounting plate. This more closely resembles a fixed boundary condition, with $K=0.5$. Comparing the results, we can approximate K_{actual} = 0.7

ANALYSIS

Simplified Beam Modeling

An approach taken by Hiller et al use a voxel-based, mass-spring lattice to simulate the dynamics of highly deformable heterogeneous materials [20]. Rather than using standard springs, beams with varying size and stiffness are used to model connection between voxels. Further simplification is possible with the physical characterization of discrete modeling elements to validate the beam modeling [19]. The software used in our analyses is a simple beam modeling software, Oasys GSA [21], used in structural engineering. Linear elastic analysis is performed, and boundary conditions are “pinned” (constrained in x,y,z translation, free in x,y,z rotation).

Currently, the force transfer between nodes relies on large contact surfaces which reduce the overall contact stress. A detailed mesh FEA model of the node may be necessary to

verify that the node does not yield before the strut under varying conditions, but this will not be performed here.

Bridge: For this structure, we look into its performance under field testing conditions (one person walking across) and the maximum capacity before failure. First, we look at the load distribution throughout the structure while the load (75kg) moves from one end to the center of the structure (as with a walking person). As shown in FIGURE 5, the first two steps have a direct load path to the ground, and thus result in a column-like usage of the lattice directly beneath the applied load. The vertical compression load is resolved into compression in diagonal struts and tension in the horizontal struts. Once there is no direct path between the applied load and boundary support; the load travels through the structure in a more complex path. Assuming loading conditions do not exceed the capacity of the structure as a whole (ie: local failure due to manufacturing defects), a local failure will result in the load being redistributed to a new load path. Catastrophic failures will be discussed later.

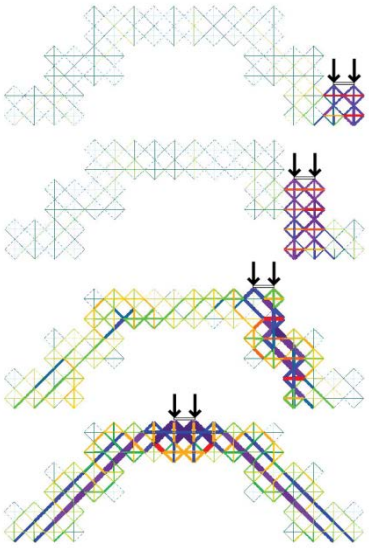

FIGURE 5: ANALYSIS RESULTS FOR MOVING LOAD ACROSS BRIDGE. BLUE INDICATES COMPRESSION, AND RED INDICATES TENSION.

Next we can analyze the performance of the structure under field testing conditions, specifically, with one person (75kg) standing at the center. Here we see that the maximum axial force is 0.1627 kN in compression. The highest tension force is 0.1116 kN.

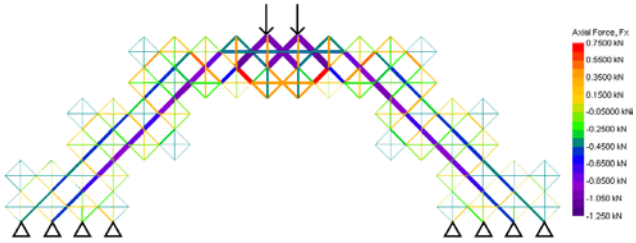

FIGURE 6: ANALYSIS RESULTS FOR LOADING UNTIL FAILURE. AXIAL FORCES IN MAXIMUM CAPACITY LOADING OF BRIDGE

When looking at the maximum capacity of this structure, we find the minimum load that causes buckling according to the derived capacity of the struts used (1.089 kN). This is 5.226 kN, or the weight of 7-8 people (FIGURE 6).

We then characterize the natural modes of the structure. The first fundamental mode is a lateral bowing of the bridge span, the second mode is a longitudinal rocking/twisting, the third mode is a lateral twisting, and the fourth mode is a longitudinal bowing. The frequencies, periods, and shapes of each mode are shown below.

TABLE II. FUNDAMENTAL MODES OF LATTICE STRUCTURE

Mode #	**Frequency (Hz)**
1st Bending (lateral)	32.72
1st Twist (longitudinal)	51.09
2nd Twist (lateral)	66.82
2nd Bending (longitudinal)	75.57

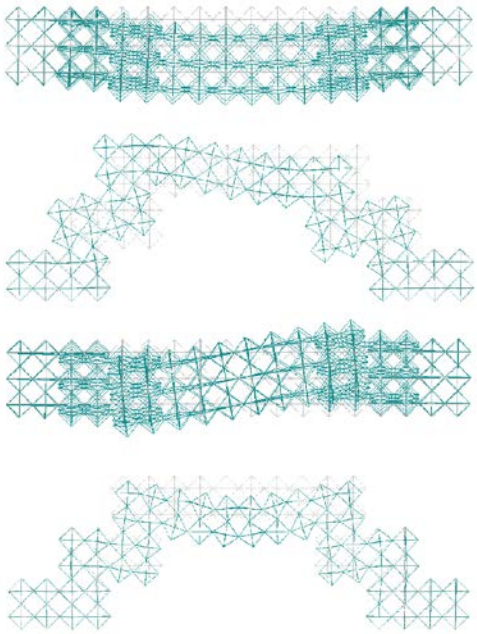

FIGURE 7: VISUALIZATION OF MODAL ANALYSIS RESULTS. (TOP TO BOTTOM)- 1ST BENDING MODE; 1ST TWISTING MODE; 2ND TWISTING MODE; 2ND BENDING MODE.

Boat: For this structure, we will look at its performance while under field testing conditions (two people floating, 150 kg total), the maximum capacity of the structure, the minimum structure required for two people, and the failure mechanisms for the structure. As expected, due to the constant pressure supplied by the surrounding buoyant force, the structure is primarily in compression (FIGURE 8).

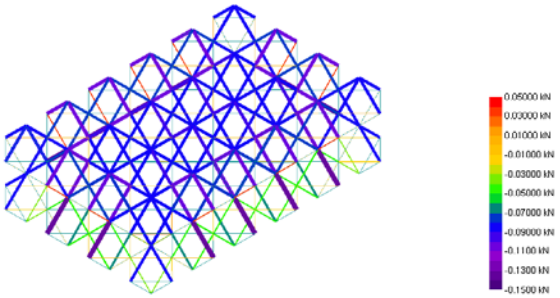

FIGURE 8: ANALYSIS RESULTS FOR TWO PERSON LOAD ON BOAT. DISTRIBUTED 150KG LOAD ON TOP, WITH BOTTOM AND SIDES SUPPORTED.

We find a maximum axial force of 0.1379 kN in compression. What would cause it to break, however, is a point load. For this given boat design, we determined the point load which would cause failure before sinking.

As described previously, due to the octahedral geometry, a load *P* applied vertically to an octahedra (oriented as shown in our structures) results in axial forces of +/- 0.35**P* in the struts. Knowing the buckling capacity of a strut then enables us to determine the critical load for the octahedra.

$$P_{cr} = P_{strut} / 0.35 = 2.857 * P_{strut} \quad (1)$$

Following (1), we determined this load to be 3.11 kN. Each voxel (including bounding box) displaces 0.02274 m^3 of water, which provides 0.227 kN of buoyant force. The minimum boat design to provide more than 3.11 kN buoyant force to prevent sinking is one with 3.11/0.227 voxels, or 13 voxels. This means a 4 x 3 x 1 boat would sink before breaking under a point load, but a 5 x 3 x 1 boat would provide enough buoyancy for a point load to break the structure (FIGURE 9).

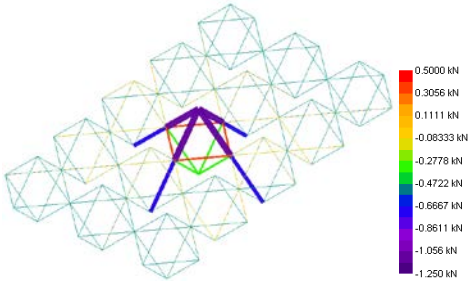

FIGURE 9: ANALYSIS RESULTS FOR POINT LOAD ON BOAT STRUCTURE. MINIMUM "FAIL BEFORE SINK" BOAT DESIGN WITH 3.11 KN LOAD

Shelter: For the shelter, we look at realistic environmental loading conditions, specifically, wind load (80 kph) and snow load (1000 N/m^2), under the assumption of a skin that can sufficiently transfer these pressure loads to the structure as point loads applied to the nodes. Wind load is found with typical wind load calculation method, which gives force *F* based on area *A*, wind pressure *P*, and drag coefficient C_d:

$$F = A \times P \times C_d \quad (2)$$

Wind pressure is found in psf by taking velocity *v* in kph, and using this equation:

$$N/m^2 = 0.00256 \times v^2 \quad (3)$$

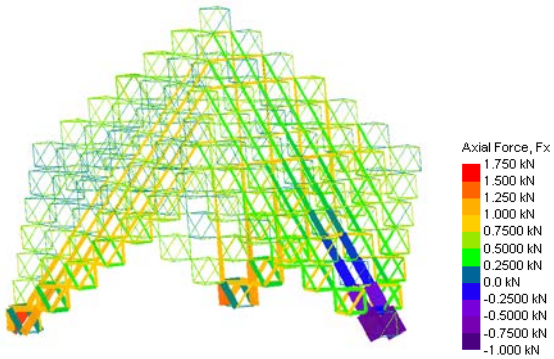

FIGURE 10: ANALYSIS RESULTS FOR WIND LOAD ON SHELTER STRUCTURE. AXIAL FORCES RESULTING FROM 80 KPH WIND LOADS

We can see here how the shelter behaves as a shell, resolving external forces into tension and compression meridional and hoop forces (FIGURE 10).

The maximum snow load is determined by member buckling. Using the maximum strut capacity and proportional voxel load, we determine the point load applied to the external voxels. From this we calculate the square footage of surface area attributed to a single voxel via tributary area, and based on this square footage determine the resulting snow load from the applied point load. We find that the maximum snow load capable with this design is 0.365m (FIGURE 11).

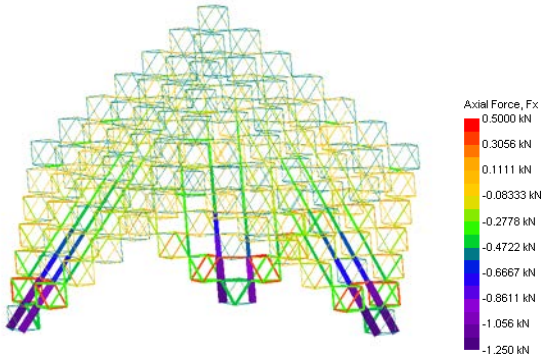

FIGURE 11: ANALYSIS RESULTS FOR SNOW LOAD ON SHELTER. AXIAL FORCES RESULTING FROM 0.365M OF SNOW LOAD RESULTING IN NEAR-BUCKLING CONDITIONS.

FIGURE 12: BUILT CASE STUDIES. L: BRIDGE (OUTLINE SHOWN DASHED) ; R-TOP: BOAT; R-BOTTOM: SHELTER

EXPERIMENTAL RESULTS

The objective for the simple case studies is to demonstrate a variety of forms with different applications and structural behaviors, while using the same base set of building blocks.

Bridge: The first case study is a 5m span bridge, capable of allowing a person to walk over some obstruction (ie: a gorge). The design is based on using "macro-blocks", a 3x2x2 (12 total) voxel assembly. The design acheives a total height of 1.7m. The width is set at 3 voxels (0.85m).The final design requires 156 voxels, which weigh 17.94 kg. Plywood panels are added to give a surface to walk on. These panels (600 x 300 x 12.7mm, 9 total) each weigh appoxmately 1.15 kg, increasing the total bridge weight to 28.3 kg. These panels are bolted onto the structure. Every boundary condition (outside facing) node is also bolted, in order to ensure that boundary struts remain captive.

Boat: After the bridge is built and tested, it is partially disassembled for transport. Four of the 12 voxel macro-bricks are then assembled together to form a 1.7 x 1.13 x 0.56m boat, weighing 5.52kg. Four plywood panels served as decking, adding an additional 4.6 kg, for a total weight of 10.12 kg. A polyethylene tarp is wrapped around the bottom and attached with elastic cords across the decking. The design is based on the buoyant force required for floating the boat with two passengers (total mass = 150 kg). At a minimum, we need 0.15 m^3 displaced, and at a depth of one-half voxel (0.15m) the buoyant force generated is 0.288kg- nearly double that required to float.

Shelter: The last case study is a shelter, sufficiently large to stand inside of, and with a large enough footprint to provide shelter for a few occupants. Using one-voxel deep panels, a three sided shelter is designed. The shelter is skinned with mylar panels attached to boundary nodes using snap rivets.

The bridge is built by a team of four people, at a rate of 5 minutes per voxel. Constructing 160 voxels takes 3.5 hours. Assembling the voxels into the bridge takes approximately 4.5 hours, for a total of 32 man hours. It takes four people two hours to partially disassemble the bridge, and two people two hours to assemble the boat, for a total of six hours. It takes two people six hours to assemble the shelter. The entire construction process, from struts to voxels to bridge to boat to shelter, takes 50 man hours.

Experimental testing

Bench testing of the voxels is challenging due to their large scale, but the behavior of the geometry and assembly strategy can be evaluated at smaller scales. Pultruded tubes do exist at smaller scales, but to reduce assembly time, the struts are cut with an abrasive waterjet from 1.6mm thick CFRP woven quasi-isotropic laminate with Young's modulus E= 9.72 GPa, which is verified experimentally using coupon tension testing. The design is modified to allow an entire strut to be cut in one operation, by incorporating end node geometry into the part. Corresponding pocket geometry for the node design is changed as well (FIGURE 13). Nodes are again injection molded. Further aspects regarding scaling are addressed later.

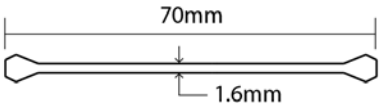

FIGURE 13: WATERJET CFRP STRUT GEOMETRY, MATERIAL THICKNESS INTO PAGE = 1.6MM.

To calculate the specific stiffness of the lattice, we build a 3x3x3 voxel cube to use in compression tests on an Instron 5985 (FIGURE 15). We applied a displacement-controlled load at a rate of 1mm/min, until failure, which occurred around 2750 N (FIGURE 14). Using the dimensions of the brick, load and displacement, we can obtain the specific elastic modulus of the lattice $E^* = 1.98$ *MPa*. Using a simulation to find this value, and we find $E^* = 1.92$ *MPa*, within 3% of the experimental value.

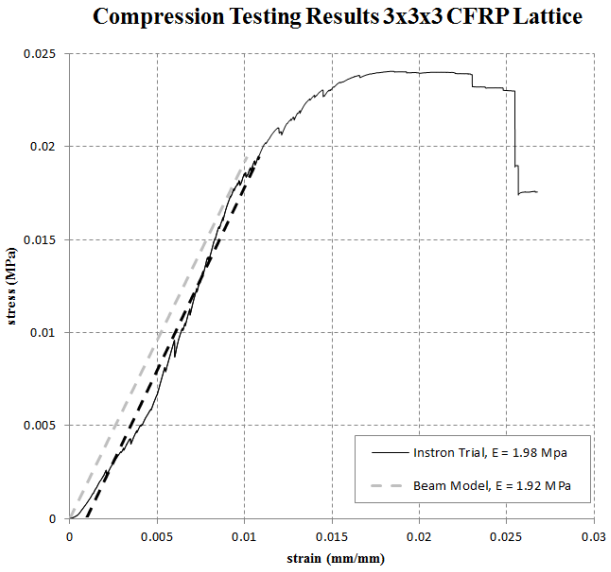

FIGURE 14: COMPARISON OF INSTRON TESTING RESULTS AND BEAM MODEL SIMULATION PREDICTIONS.

We can also extract data from the simulation to make some hypotheses about the behavior of the structure. Looking at the axial forces in the struts, find that the maximum axial force in compression is 150 N (FIGURE 14). Using the Euler buckling equation, we can calculate k, the effective column length factor. We find $k = 0.591$ which is between our predicted k factor from initial strut testing (0.7) and $k = 0.5$, which is used when both ends are fixed in all 6 degrees of freedom. This is attributable to node design. While the nodes were designed primarily for assembly, their ability to constrain the ends of the struts reduces their effective column length, thus increasing their buckling capacity. This arguably can make the structure stiffer. However, the additional mass in the node must be included when calculating the specific density of the structure, which reduces the density-specific stiffness E^*/ρ^*.

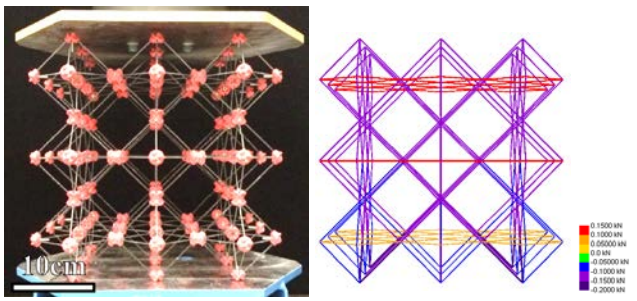

FIGURE 15: (L) 3x3x3 VOXEL TEST SPECIMEN BETWEEN TWO PLATES FOR INSTRON TESTING, (R) BEAM MODELING RESULTS FOR LOAD AT FAILURE P = 2750 N.

The values derived from the compression testing can be used to determine the power scaling law value, a, for cellular solids, from [3]. The ratio of macroscopic stiffness E^* and material stiffness E are related to the ratio of cellular solid density ρ^* and material density ρ through a power law, $E^*/E \approx b(\rho^*/\rho_s)^a$, where b depends on the direction of the applied load. For our case, we will use $b = 1/3$ [3]. We find that $a = 1.65$, which is close to other reported values for this lattice geometry [17][19]. We can use this value to estimate the expected stiffness of the larger pultruded carbon fiber structure. Here we find $E^* = 2.73$ *MPa*, which isn't much stiffer, but it is at roughly 1/3 of the density. FIGURE 16 compares these results to other reported results.

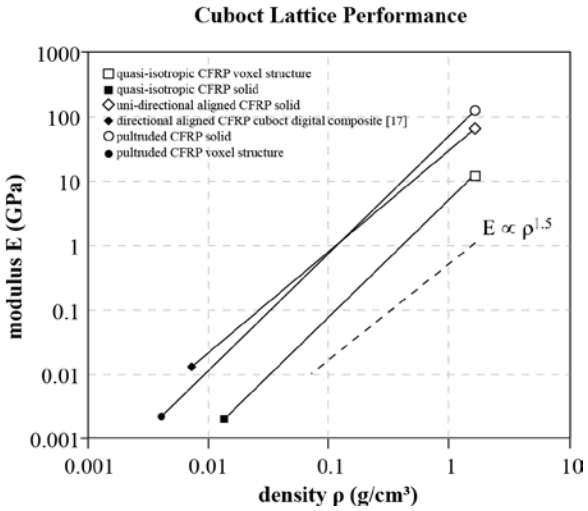

FIGURE 16: COMPARISON OF SPECIFIC MODULUS AND SPECIFIC DENSITY OF VARIOUS CUBOCT LATTICE STRUCTURES.

While we have determined E^*, it is difficult to assess its performance as an actual structure under loading with just this value. Here we wish to find specific bending stiffness E^*I, which will allow us to compare our structure to other lightweight structures with normalized metrics.

A 3x3x6 voxel beam is built using a similar approach to the larger structures, using M3 nuts and bolts (FIGURE 17). It is bolted mounted to an aluminum bracket, which is bolted to an optical table. Loads are then applied at the tip, and deflection is measured using a Mitutoyo electronic height gage. The beam length is L = 0.68m. The loads applied are 0.5, 1.0, 1.5, 2.0, 2.5, 3.0, 3.5, 4.0, 4.5 and 5.0 kg, with deflections of 0.5, 0.86, 1.36, 1.88, 2.34, 2.75, 3.32, 3.77, 4.25, and 4.64 mm, respectively. Using $EI = FL^3/3y$, we find the average bending stiffness of our beam to be E^*I = 1362 N·m^2. This experiment is also simulated, and we find E^*I to be 1467 N·m^2, a difference of around 7%. This is attributable to the loading scenario and boundary conditions. Bending will result in compression on the bottom chord and tension on the top chord. The external node distances are not constrained by a skin or additional struts, and the node between adjacent voxels is left to enforce this distance. In the compression test, the only boundary condition deformation is normal to the boundary surface (expansion as a Poisson effect), and this is constrained by the struts connected to the node.

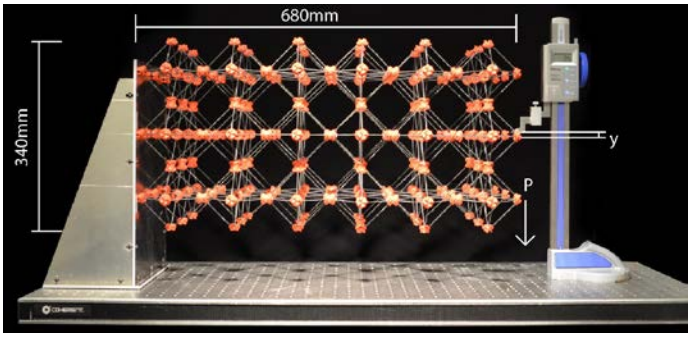

FIGURE 17: BENCHTOP TEST SETUP OF 3x3x6 CFRP VOXEL BEAM WITH MOUNTING BRACKET, OPTICAL TABLE, AND HEIGHT GAGE

When we simulate the bending stiffness of the pultruded tube lattice, using the same 3x3x6 voxel beam, We find E^*I = 570,000 N·m^2. This is several orders of magnitude larger than the solid CFRP lattice and an order of magnitude lower in specific density. This is attributable to the use of hollow tubes, which add a level of hierarchy to the structure. This agrees with the trend of hierarchical structures being more mass efficient for lightly loaded space applications [22].

EVALUATION

The bench top analysis and simulation allows moving from E^* to E^*I, which is a common value shown for beams and masts. Given the light to ultra-light weight of these structures, one application that is worth discussing and evaluating is in space structures. Structures such as deployable booms, unfurling satellite dishes, and erectable truss structures face strict requirements during launch [23]. Launch vehicles are limited by both the mass and volume of the payload they can carry, and the forces that these payloads undergo (10's of G's) are orders of magnitude greater than the forces they will experience on orbit under microgravity. As a result, mass and volume are lost to structures over engineered for their final purpose on orbit.

Deployable structures have some of the highest stiffness to weight ratios [24], and their mass-specific structural performance has been documented extensively [25]. Because the modular system we propose can be built to arbitrarily large sizes, it is appealing as a solution for space structures larger than what can fit in a launch vehicle. In FIGURE 18 we compare our structure to existing space structures, and we will suggest ways to compete with and surpass these structures.

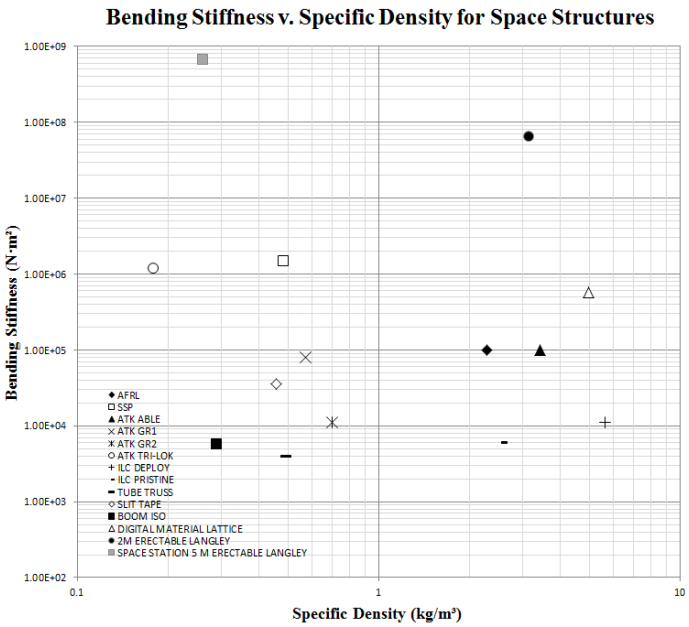

FIGURE 18: BENDING STIFFNESS V DENSITY OF SPACE STRUCTURES AND DIGITAL MATERIAL STRUCTURES. DATA FOR SPACE STRUCTURES OBTAINED FROM [24][25]

Our structure is above the mean bending stiffness, but is the second highest specific density. We can improve this, while maintaining competitive bending stiffness. One is to increase lattice pitch and strut diameter. Increasing lattice pitch will increase the I of the beam. However, it will also lower the load capacity of the strut. This can be counteracted by also increasing the I of the strut. In this way, the hierarchical design can be leveraged to make a light and stiff structure.

DISCUSSION

The flexibility in this modular structural system comes from the interplay of several variables: lattice topology, lattice pitch, strut cross section, and base material. Each of these is a deep research topic, but we will touch on several key aspects here. Lattice topology refers to the geometric configuration of the lattice base cell, including number of elements and

orientation. By changing topology, the lattice topology scaling factor a changes, which affects how ρ^* and E^* are related. Our topology, the cuboctohedra, differs in a from other lattices, such as the octet and kelvin lattice, with a's of 1 and 2, respectively. The implications of lattice choice also impact structural requirements and manufacturing constraints. The research of the design-space of these choices is ongoing.

Lattice pitch, or strut length, essentially determines scale. This may have the largest implications. Scaling down to mm-scale pitch requires micro-machining and micro-assembly. While the mechanical properties are still relevant, the challenge in assembly is significant. At this scale, most approaches use additive manufacturing [16]. However, these structures cannot be reconfigured, and are limited in overall size to the machine print size. Scaling up also introduces challenges. Pultruded tubes come in meter-diameter and larger, and the length can be decomposed into partial interlocking tubes. However, at this scale, manipulation in a gravity environment becomes nearly impossible. That is why many proposals for structures built from struts ranging from 10^0 to 10^2 m have been for extra-large space structures [26], where the microgravity environment would allow such scales to be built. The assembly itself, as automation is desirable at most scales and mandatory for large scales [27]. These structures face other constraints previously mentioned, such as optimizing for mass and volume within launch shrouds.

Lastly, material selection is also a variable, as heterogeneous voxels can be joined to form continuum structures with unique properties. For example, local failures of composite struts could lead to a domino-effect of overloading and failures. Mechanisms for dealing with catastrophic yielding of the structure should be devised prior to large scale application. This could be alternating between composite voxels and voxels made from a material with post-yield capacity, such as steel, which could temporarily prevent total collapse.

CONCLUSION

Digital materials are modular, reconfigurable cellular structures that exhibit high performance with flexibility for a variety of applications. We describe a construction methodology based on specific geometric and mechanical relationships that ensure local and global behaviors are coordinated to express desired structural properties. The design variables present a wide range of design choices that allow tuning of structural performance and other properties

ACKNOWLEDGEMENT

We would like to thank Angelica Chavez for her contributions to the construction and documentation of the structures. We would also like to thank Holly Jackson for her contributions to the research and design of lattice structures for space applications. Lastly we would like to acknowledge Joseph Kim for his significant contributions to the construction of struts and voxels.

REFERENCES

[1] M. Yim, D. G. Duff, and K. D. Roufas, "PolyBot: a modular reconfigurable robot," *Proc. 2000 ICRA. Millenn. Conf. IEEE Int. Conf. Robot. Autom. Symp. Proc. (Cat. No.00CH37065)*, vol. 1, pp. 514–520, 2000.

[2] C. Y. Baldwin and K. B. Clark, *Design Rules: The Power of Modularity Volume 1*, vol. 26. 2000.

[3] M. F. Ashby, "The properties of foams and lattices.," *Philos. Trans. A. Math. Phys. Eng. Sci.*, vol. 364, no. 1838, pp. 15–30, 2006.

[4] R. Lakes, "Materials with structure hierarchy," *Nature*, vol. 361, pp. 511–515, 1993.

[5] J. Chilton, *Space Grid Structures*. Achitectural Press, 2000.

[6] A. D. Marchese, C. D. Onal, and D. Rus, "Autonomous Soft Robotic Fish Capable of Escape Maneuvers Using Fluidic Elastomer Actuators," *Soft Robot.*, vol. 1, no. 1, pp. 75–87, 2014.

[7] J. Gerdes, A. Holness, A. Perez-Rosado, L. Roberts, A. Greisinger, E. Barnett, J. Kempny, D. Lingam, C.-H. Yeh, H. a. Bruck, and S. K. Gupta, "Robo Raven: A Flapping-Wing Air Vehicle with Highly Compliant and Independently Controlled Wings," *Soft Robot.*, vol. 1, no. 4, pp. 275–288, 2014.

[8] M. Manti, T. Hassan, G. Passetti, N. D'Elia, C. Laschi, and M. Cianchetti, "A Bioinspired Soft Robotic Gripper for Adaptable and Effective Grasping," *Soft Robot.*, vol. 2, no. 3, pp. 107–116, 2015.

[9] K. a. Faist and G. J. Wiens, "Parametric study on the use of Hoberman mechanisms for reconfigurable antenna and solar arrays," *IEEE Aerosp. Conf. Proc.*, 2010.

[10] F. Nigl, S. Li, J. E. Blum, and H. Lipson, "Structure-reconfiguring robots: Autonomous truss reconfiguration and manipulation," *IEEE Robot. Autom. Mag.*, vol. 20, no. 3, pp. 60–71, 2013.

[11] Y. Terada and S. Murata, "Automatic assembly system for a large-scale modular structure - hardware design of module and assembler robot," *2004 IEEE/RSJ Int. Conf. Intell. Robot. Syst. (IEEE Cat. No.04CH37566)*, vol. 3, pp. 2349–2355, 2004.

[12] J. Neubert and H. Lipson, "Soldercubes: a self-soldering self-reconfiguring modular robot system," *Auton. Robots*, vol. 1, no. 20, 2015.

[13] a. Spröwitz, R. Moeckel, M. Vespignani, S. Bonardi, and a. J. Ijspeert, "Roombots: A hardware perspective on 3D self-reconfiguration and locomotion with a

homogeneous modular robot," *Rob. Auton. Syst.*, vol. 62, no. 7, pp. 1016–1033, 2014.

[14] S. Murata, H. Kurokawa, E. Yoshida, K. Tomita, and S. Kokaji, "A 3-D self-reconfigurable structure," *Proc. Int. Conf. Robot. Autom.*, vol. 1, pp. 432–439, 1998.

[15] L. Gibson, *Cellular Solids: Structure and Properties*. Cambridge University Press, 1999.

[16] X. Zheng, H. Lee, T. H. Weisgraber, M. Shusteff, J. DeOtte, E. B. Duoss, J. D. Kuntz, M. M. Biener, Q. Ge, J. a Jackson, S. O. Kucheyev, N. X. Fang, and C. M. Spadaccini, "Ultralight, ultrastiff mechanical metamaterials.," *Science*, vol. 344, no. 6190, pp. 1373–7, 2014.

[17] K. C. Cheung and N. Gershenfeld, "Reversibly assembled cellular composite materials.," *Science*, vol. 341, no. 6151, pp. 1219–21, 2013.

[18] K. J. Bathe, *The Mechanics of Solids and Stuctures - Hierarchical Modeling and the Finite Element Solution*. Springer, 2011.

[19] S. Calisch, "Physical Finite Elements," Massachusetts Institute of Technology, 2014.

[20] J. Hiller and H. Lipson, "Dynamic Simulation of Soft Multimaterial 3D-Printed Objects," *Soft Robot.*, vol. 1, no. 1, pp. 88–101, 2014.

[21] "GSA." [Online]. Available: http://www.oasys-software.com/products/engineering/gsa-suite.html.

[22] T. Murphey and J. Hinkle, "Some performance trends in hierarchical truss structures," in *44th AIAA/ASME/ASCE/AHS Structures, Structural Dynamics, and Materials Conference*, 2003.

[23] L. Puig, A. Barton, and N. Rando, "A review on large deployable structures for astrophysics missions," *Acta Astronautica*, vol. 67, no. 1–2. pp. 12–26, 2010.

[24] M. M. Mikulas, T. J. Collins, W. Doggett, J. Dorsey, and J. Watson, "Truss performance and packaging metrics," in *AIP Conference Proceedings*, 2006, vol. 813, pp. 1000–1009.

[25] T. Murphey, "'Booms and Trusses,'" in *Recent Advances in Gossamer Spacecraft*, 2006, pp. 1–43.

[26] H. Bush and M. Mikulas, "Some Design Considerations for Large Space Structures," in *AIAA/ASME 18th Structures, Structural Dynamics, and Materials Conference*, 1977.

[27] M. Mikulas and H. Bush, "Design, Construction, and Utilization of a Space Station Assembled from 5-Meter Erectable Struts," *NASA Struct. Interact. Technol.*, 1987.